

# How to estimate the differential acceleration in a two-species atom interferometer to test the equivalence principle

G. Varoquaux<sup>1‡</sup>, R.A. Nyman<sup>1§</sup>, R. Geiger<sup>1</sup>, P. Cheinet<sup>1</sup>, A. Landragin<sup>2</sup> and P. Bouyer<sup>1</sup>

<sup>1</sup> Laboratoire Charles Fabry de l'Institut d'Optique, Campus Polytechnique, RD 128, 91127 Palaiseau, France

<sup>2</sup> LNE-SYRTE, UMR8630, UPMC, Observatoire de Paris, 61 avenue de l'Observatoire, 75014 Paris, France

PACS numbers: 37.25.+k, 03.75.Dg

## Abstract.

We propose a scheme for testing the weak equivalence principle (Universality of Free Fall) using an atom-interferometric measurement of the local differential acceleration between two atomic species with a large mass ratio as test masses. A apparatus in free fall can be used to track atomic free-fall trajectories over large distances. We show how the differential acceleration can be extracted from the interferometric signal using Bayesian statistical estimation, even in the case of a large mass and laser wavelength difference. We show that this statistical estimation method does not suffer from acceleration noise of the platform and does not require repeatable experimental conditions. We specialize our discussion to a dual potassium/rubidium interferometer and extend our protocol with other atomic mixtures. Finally, we discuss the performances of the UFF test developed for the free-fall (0-g) airplane in the ICE project (<http://www.ice-space.fr>).

Submitted to: *New J. Phys.*

‡ Present address: Laboratoire de Neuroimagerie Assistée par Ordinateur, CEA/SAC/DSV/I2BM/NeuroSpin, 91191 Gif-sur-Yvette, France

§ Present address : Centre for Cold Matter, Blackett Laboratory, Imperial College, London, SW7 2BW, United Kingdom

## 1. Introduction

The Einstein equivalence principle is fundamental to the standard model of particle physics and all metric theories of gravity [1, 2]. It can be broken into three elementary principles: the local Lorentz invariance; the local position invariance (also known as universality of red shift); and the universality of free-fall (UFF), stating that all freely-falling point particles follow identical trajectories independent of their internal composition. The Lorentz invariance and the position invariance are local properties and can be tested to unmatched precision using atomic clocks [3, 4, 5] and ultra-stable cavities [6]. On the contrary, the UFF can only be tested by tracking trajectories, ideally of freely-falling test masses. Various extensions to the current theoretical-physics framework predict violations of the UFF [7]. It is thus important to look experimentally for such violations and push the limits of experimental tests of the UFF. Moreover, laboratory experiments are an important complement to astrophysical observations in testing fundamental physics, because of the possibility of controlling the environment and repeating the experiments in varying conditions.

In this article, we show that using an atom interferometer with two different atomic species in free fall can lead to an accurate test of the UFF, even for different laser wavelength and mass (i.e. different scaling factors for the interferometers). We present a protocol that allows us to accurately extract the acceleration difference and show that this measurement is almost insensitive to strong vibrational noise or platform movement, which usually limit the atom interferometer accuracy, or platform movement. We show how Bayesian statistical methods introduced in [9] for two identical atom interferometers can be extended to extract the acceleration difference between the two atomic species, taking advantage of phase-correlated measurements between both interferometers. For the sake of clarity, we focus on the simultaneous use of rubidium 87 and potassium 39 atoms in a light-pulse gravimeter [8]. Comparing the acceleration of these two different atomic species constitutes a meaningful test of the UFF, as they combine a large mass ratio (almost a factor of two), very different nuclear compositions (37 protons and 50 neutrons for  $^{87}\text{Rb}$  and 20/19 for  $^{39}\text{K}$ ) and almost equal laser wavelength and thus interferometer scale factors. We show that, with reasonable experimental parameters, a test could reach the accuracy of  $\eta \sim 5 \cdot 10^{-11}$  in a one-day parabolic flight campaign in a zero-g airplane, and, if extended to long-duration experiments, could compete with the best available apparatus. Our discussion can be generalized to other atomic species such as the mixture proposed in [10] or lighter atomic species.

## 2. Testing the Universality of Free-Fall

A figure of merit often used to characterize a test of the UFF is the Eötvös ratio  $\eta$ , giving the fractional difference in acceleration between two test masses in free-fall:  $\eta = \Delta a/a$ . Alternate quantum gravitation theories predict deviations from the UFF for  $\eta \lesssim 10^{-13}$  [11, 12, 13]. Current experimental limits on violations of the UFF ( $\eta < 10^{-13}$ ) are set

by lunar laser-ranging measurements [14] and torsion-balance laboratory experiments [15]. Tests of the UFF by monitoring the acceleration difference between two objects freely falling simultaneously have shown  $\eta < 10^{-10}$  [16]. While all these experiments test the validity of the UFF on macroscopic objects, in the quest for a quantum gravity theory, it is interesting to look for deviations on elementary, or microscopic, particles, where quantum mechanics is needed to describe their evolution [17, 18].

The accuracy and sensitivity of local-acceleration measurements using atom-interferometry nowadays rival state-of-the-art conventional accelerometers using macroscopic test masses [8, 19, 20]. With such sensors, the quantity measured directly relates to the acceleration of weakly-interacting particles via experimentally well-controlled quantities, such as laser wavelengths [21]. In addition, the evolution of these particles in the gravitational field can be modeled within a covariant quantum field theory [22]. Recent results using atom-interferometric gravimetry to compare the acceleration between two isotopes [19, 23] have demonstrated the possibility of atom-interferometric tests of the UFF. Ongoing efforts to extend the size of inertial-sensing atom interferometers by increasing the interrogation time [24, 10, 25] open the door to high-accuracy atom accelerometers which will be very sensitive to smaller accelerations, thus pushing the limits of these tests. These long interrogation times, i.e. large free-fall heights, can be achieved when using a large experimental chamber to launch the atoms such as a ten-meter-high fountain, as suggested in [10].

Compact apparatuses can also be used in reduced-gravity environments, such as drop towers [26, 27], orbital platforms [28], or atmospheric parabolic flight [25]. However, increasing the interrogation time also increases the sensitivity of the interferometer to acceleration noise [29] which can scale from  $\sim 10^{-5} \text{ m.s}^2$  in drop towers to  $\sim 10^{-2} \text{ m.s}^2$  in the 0-g Airbus [30] and on the International Space Station [31]. Atoms, isolated in a vacuum chamber, are truly in free-fall in the Earth's local gravity field, as long as they do not hit the chamber walls, or experience field gradients (optical or static magnetic). However, their acceleration is recorded relative to an ill-defined experimental frame. This can compromise the increase in sensitivity. Measuring differential phase between similar interferometers using the same light has been shown to reject common-mode inertial noise up to large scaling-factors [32, 33, 34], however, in the case of an UFF measurement, the two interferometers compared do not share the same sensitivity to inertial effects and the common-mode rejection is not straightforward.

### 3. Differential atom interferometer in free-fall

The acceleration-measurement process on each single species can be pictured as marking successive positions of freely-falling atoms with a pair of Raman lasers, pulsed in time. The resulting atomic phase shift  $\phi$  is the difference between the relative phase of the Raman lasers at the atom's successive classical positions [19, 35]. When the Raman lasers are used in a retroreflected configuration, this phase simply relates to the distance between the atomic cloud and the reference retroreflecting mirror. In such a three-pulse

interferometer, using atoms without initial velocity, the inertial phase shift varies with the acceleration  $a$  as:

$$\phi = k a T^2, \quad (1)$$

where  $a$  is the acceleration of the atoms relative to the mirror,  $k$  is the effective wavevector of the Raman lasers, and  $T$  is the time between successive pulses.

To test the UFF, we need to extract the difference in acceleration between the two species. However, in atom interferometers with internal-state labeling [21], the experimental signal is the population ratio  $n$  between the two output arms of a single interferometer  $n \sim \cos(\phi + \Phi)$ , with  $\Phi$  related to the phase noise of the Raman lasers [24] and contributions due to vibrations and unwanted inertial effects on the retroreflecting mirror [36]. To extract an absolute value of the interferometric phase, accumulating data to scan a fringe is required. This accumulation of several experimental points can thus be hindered by the acceleration noise of the platform, as the acceleration measured may vary from one measurement to another. To have access to long integration, we thus want to extract as much information as possible about the phase difference with a minimum set of independent measurements.

We now focus on the Potassium(K)-Rubidium(Rb) atom interferometer described in [24]. The UFF experimental signal that we are interested in is the Eötvös ratio,  $\eta = 2(a_K - a_{Rb})/(a_K + a_{Rb})$  with  $a_K$  and  $a_{Rb}$  the accelerations of potassium and rubidium. We thus want to extract the acceleration difference  $\delta a = a_K - a_{Rb}$ . This can be related directly to the difference of the inertial phase of each interferometer: using Equation (1),  $\delta\phi = \phi_K - \phi_{Rb} = k_K a_K T_K^2 - k_{Rb} a_{Rb} T_{Rb}^2$  where  $k_K = 4\pi/767 \text{ nm}^{-1}$  and  $k_{Rb} = 4\pi/780 \text{ nm}^{-1}$  are the effective wave-vectors of the Raman transitions, and  $T_K$  and  $T_{Rb}$  are the interrogation times for the K and Rb interferometers respectively. In order to directly read out  $\delta a$ , we need to adjust the respective interferometer interrogation times so that they have the same scale factor:  $k_{Rb} T_{Rb}^2 = k_K T_K^2 = \mathcal{S}$ , i.e.  $T_{Rb}/T_K \sim 1.008$ . In this case, we simply have

$$\delta\phi = \mathcal{S}\delta a. \quad (2)$$

As in [9] we make a statistical description of the measurement process in a two-species interferometer. Two quantities are measured:

$$\begin{cases} n_K = A + B \cos(\phi_K + \Phi_K) \\ n_{Rb} = C + D \cos(\phi_{Rb} + \Phi_{Rb}) \end{cases} \quad (3)$$

where the capital letters represent fluctuating quantities:  $A$  and  $C$  are the offsets of the population measurement,  $B$  and  $D$  are the fringe visibilities, and  $\Phi_K$  and  $\Phi_{Rb}$  are related to the phase and acceleration noises on the two interferometers. In the following, we neglect the laser-induced phase noise, due e.g. to finite laser linewidth [37] or microwave source jitter [24], since it can be reduced with appropriate phase-locking techniques [36].

The interferometric phase noise, due to vibrations or other uncontrolled inertial effects, appears as shifts of the local Raman phase for each interferometer. Following

[38] and assuming a white acceleration noise of power spectral density (PSD)  $S_\alpha^0$ , the standard deviation of  $\Phi_{\text{K,Rb}}$  can be written

$$\sigma_{\Phi_i} = k_i T_i^{3/2} \sqrt{\frac{2S_\alpha^0}{3}}, i = \text{K, Rb}. \quad (4)$$

This phase noise can be expressed as a random spatial displacement  $X(t)$  of deviation  $\sigma_X = \sigma_\Phi/k$  of the retroreflecting mirror. The effect of other common-mode, spatial, Raman-phase fluctuations such as optical aberrations [39] can also be included in this fluctuating variable  $X$ .

When calculating the differential response of the two-species atom interferometer, the relative phase noise between the two interferometers can be written  $\Delta\Phi = \Phi_{\text{K}} - \Phi_{\text{Rb}} = k_{\text{K}} \tilde{X}$  where the standard deviations of  $\tilde{X}$  and  $X$  are simply related by a vernier-scale relation

$$\sigma_{\tilde{X}} = \sigma_X \frac{\delta k}{2k} \quad (5)$$

with  $\sigma_X$  calculated for  $T = T_{\text{K}}$  and  $\delta k/2k = (k_{\text{K}} - k_{\text{Rb}})/2k_{\text{K}} \approx 8.5 \cdot 10^{-3}$ . The derivation of this scale relation and its physical explanation are detailed in Appendix B. We can now rewrite Eq. (3) as a simplified measurement model, highlighting differential effects:

$$\begin{cases} n_{\text{K}} = A + B \cos(\tilde{\Phi}_{\text{Rb}} + \delta\phi + k_{\text{K}} \tilde{X}) \\ n_{\text{Rb}} = C + D \cos \tilde{\Phi}_{\text{Rb}} \end{cases} \quad (6)$$

The phase  $\tilde{\Phi}_{\text{Rb}} = \mathcal{S}a_{\text{Rb}} + \Phi_{\text{Rb}}$  of the rubidium interferometer is taken as the reference. The phase offset in the potassium interferometer includes the UFF signature,  $\delta\phi$  and the effect of vibrations of the retroreflecting mirror,  $k_{\text{K}} \tilde{X}$ .

#### 4. Extracting the differential phase using Bayesian analysis

To extract the differential phase  $\delta\phi$  from statistically independent data acquired during different measurement sequences, we use recursive Bayesian estimation [40, 41]. Although several solutions for signal processing in atom-interferometric inertial sensors have been studied [9, 42], Bayesian estimators make best use of a noise model for estimating information from experimental data [9] and they have been successfully used in quantum optics [41, 43] or in optical interferometers [44]. Moreover, Kalman filtering, a restricted version of Bayesian estimation, plays a critical role for proper use of fiber-optic gyroscope data [45]. In the Bayesian framework, the parameters to be estimated are considered as random variables, whose probability distribution is deduced from the measurements by inverting the measurement model. Using Bayes' theorem, we calculate the probability distribution function  $p(\delta\phi | (n_{\text{K}}, n_{\text{Rb}})_i)$  for the parameter  $\delta\phi$  given the results of a coupled measurement on both interferometers  $(n_{\text{K}}, n_{\text{Rb}})_i$ , for each measurement  $i$ . The probability distribution  $p(\delta\phi | (n_{\text{K}}, n_{\text{Rb}})_1, (n_{\text{K}}, n_{\text{Rb}})_2, \dots)$  for  $\delta\phi$ , given all measurements, is the product of all these conditional probabilities:

$$p(\delta\phi | (n_{\text{K}}, n_{\text{Rb}})_1, (n_{\text{K}}, n_{\text{Rb}})_2, \dots) = p(\delta\phi | (n_{\text{K}}, n_{\text{Rb}})_1) p(\delta\phi | (n_{\text{K}}, n_{\text{Rb}})_2) \dots \quad (7)$$

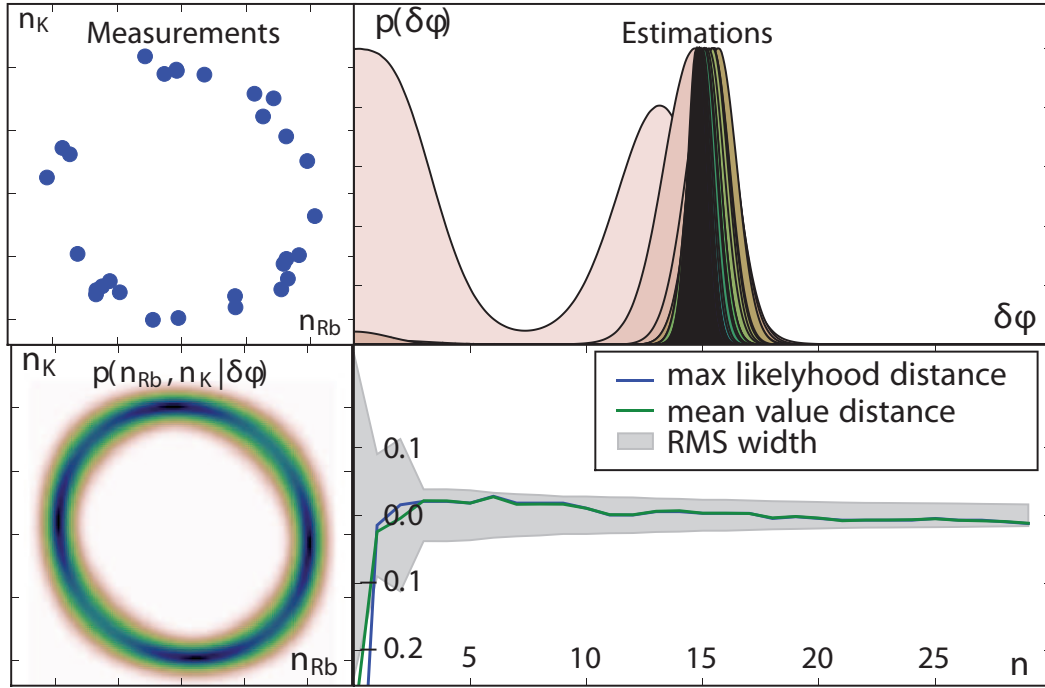


**Figure 1.** Simulation of the model of Eq. (6). The random variable  $\tilde{\Phi}_{Rb}$  is generated from a uniform distribution taken in the interval  $0, 2\pi$ . We generate  $X$  from a normal distribution centered around 0 with  $\sigma_X = 1.2 \mu\text{m}$ .  $A, B, C$  and  $D$  are generated from a normal distribution with  $\sigma = 0.05$ . The mean values are 0 for  $A$  and  $C$  and 1 for  $B$  and  $D$ . For each simulation are displayed (going clockwise, starting bottom left) : the measurement probability in the  $(n_{Rb}, n_K)$  plane for the value of the hidden parameter  $\delta\phi$  choosen in the simulation, the different measurements actually drawn, the successive probability-distribution estimations for  $\delta\phi$ , and the distance between estimated values of  $\delta\phi$  and the actual value.

The non linearities of the measurement model introduced by the trigonometric functions in Eq. (6), with different periods  $k_{Rb}$  and  $k_K$ , make the analytical calculation of the conditional probability required for the Bayesian estimation tedious and the resulting expression is computationally costly to evaluate. We calculate this probability distribution (i.e. the “posterior”) by using Monte Carlo sampling of the state space with the noise model (Eq. (6)). We use the probability law to estimate the reversed conditional probability (i.e. the “prior”)  $p(n_K, n_{Rb} | \delta\phi)$ . A kernel density estimator [40] can be used to reduce the number of sampling points required, though this may not increase overall numerical efficiency. The posterior, used for Eq. (7), is obtained from the prior using Bayes’ theorem [46].

We have run Monte Carlo simulations of the estimation process for different values of displacement noise amplitude  $\sigma_X$  with the measurement model described in Eq. (6), as pictured in figure 1. We use Gaussian noise of standard deviation  $\sigma = 0.05$  for the various parameters. The common-mode phase  $\tilde{\Phi}_{Rb}$  is taken to be uniformly random in the interval  $[0, 2\pi]$ . As seen in figure 2, the estimator converges to a precise value of the

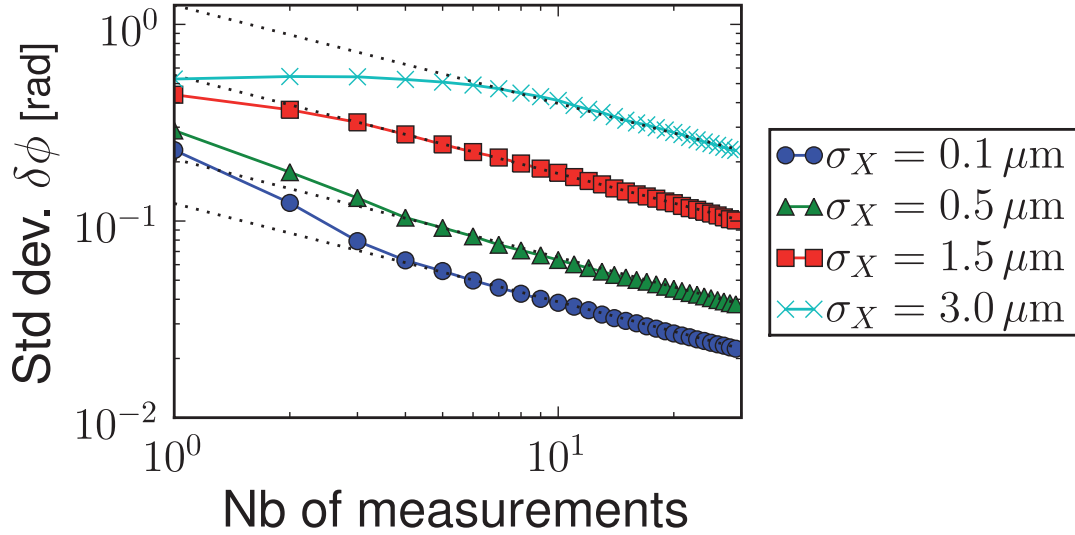


**Figure 2.** Standard deviation of the Bayesian estimation of the differential phase  $\delta\phi$  between K and Rb interferometers. The standard deviations of the estimation of the differential phase decrease at different rates with repeated measurements for different mirror-displacement amplitudes (dotted lines). The convergence of the points towards the dotted lines shows how correlated noise is handled by the algorithm.

differential phase with fewer than 10 uncorrelated measurements for fluctuations of  $X$  up to a few micrometers, which corresponds to a drift of the one-species interferometric signal by several complete fringes. This surprising result comes from the vernier scale relation in Eq. (5) that reduces the differential measurement sensitivity to Raman-phase fluctuations.

One should note that if  $\delta\phi \sim 0$ , the measurements performed do not contain enough information for good estimation (we have checked that the Fisher information matrix [40] is zero for  $\delta\phi = 0$ ). This can be easily understood since the data  $n_K$  and  $n_{Rb}$  are then distributed along a single line and we lose the sensitivity to phase/vibration noise [42]. It is thus necessary to introduce a controlled phase jump of  $\pi/2$  in one of the two interferometers, e.g. on the phase of the Raman lasers. This choice of interferometric phase shift corresponds to working on the side of a fringe in a standard interferometer: the two parameters are maximally independent, distributed on a large-ellipticity curve rather than a flat line (see figure 1), giving optimal measurement sensitivity.

We have performed other simulations for different choices of noise distribution for  $X$ , which can be related to acceleration-noise power spectral density using the interferometer sensitivity function as described in Appendix B. We find that the convergence rate is not dependent on the nature of the bell-shaped noise distribution, nor on its behavior in its wings, but only on the RMS amplitude of the fluctuations. In addition, we have performed simulations for different dual-interferometer configurations in which the distance between the effective Raman transition wave vectors is reduced, thus reducing the Vernier-scale effect. Specifically we have investigated using the potassium D1 transition (at 770 nm) with rubidium, or the two isotopes of rubidium,

	K-D2/Rb	K-D1/Rb	<sup>85</sup> Rb/ <sup>87</sup> Rb
$\sigma_X \sim 0.1 \mu\text{m}$	.022	.022	.021
$\sigma_X \sim 0.5 \mu\text{m}$	.037	.033	.021
$\sigma_X \sim 1.5 \mu\text{m}$	.101	.075	.021
$\sigma_X \sim 3.0 \mu\text{m}$	.229	.166	.022

**Table 1.** Standard deviation on the phase estimate, in radians, after 30 measurements, for different mirror-displacement amplitudes  $\sigma_X$ , and for different pairs of Raman transitions. The species and transition lines considered here are: the potassium D2 line at 767 nm, the potassium D1 line at 770 nm, and the rubidium 85 and 87 D2 lines at 780 nm, with a distance of 3 GHz  $\sim$  0.03 nm between the two isotopes.

with transitions separated only by 3 GHz  $\sim$  0.03 nm (see tab. 1). We find that for small variations of  $X$ , ( $\sigma_X < 0.5 \mu\text{m}$  typ.), the phase-estimation is not limited by the Vernier scale effect as the convergence speed is similar for all three interferometer configurations.

## 5. Higher-order inertial effects

We now consider the contribution of additional inertial effects on the differential measurement strategy. Equation (1) gives only dependence of the phase shift to an acceleration, and does not include rotation, gravity gradients, and higher-order effects. The effect of rotation can, in principle, be rejected by a feed-forward on the phase of the lasers [47] and a accurate control of the atom cloud velocity after release. We are then left with the major second-order contribution to the phase shifts, the effect of the gravity gradients. Since the atomic trajectories in the two interferometers explore slightly different altitudes, gravity gradients will add a contribution to the inertial phase shift [48, 49]:

$$\phi_\gamma \sim k \gamma T^2 \left( \frac{7}{12} T^2 a - \left( v - \frac{v_r}{2} \right) T \right), \quad (8)$$

where  $v$  is the relative velocity between the center of mass of the atom cloud and the reference mirror.  $v_r = \frac{\hbar k}{m}$  is the recoil velocity and  $\gamma$  the gravity gradient. If the scale factors  $\mathcal{S}$  of both interferometers are kept constant, the numerical value of the total differential phase shift (Eq. 2) then becomes  $\delta\phi_{\text{tot}} = \delta\phi + \delta\phi_\gamma$  with  $\delta\phi_\gamma$  the residual gradient-induced phase shift. In general, the contribution to  $\delta\phi_\gamma$  of first term in Eq. (8) is negligible and  $v$  can be chosen to compensate for the recoil velocity  $\hbar k/m$ .

## 6. Conclusion

We finally turn to the specific case of the experiment in the 0-g airplane described in [25]. We can use the results from our simulation to give an order of magnitude of the precision achievable by a campaign of measurements in Zero-G flights. For a residual displacement from free fall  $X$  such as  $\sigma_X \sim 1 \mu\text{m}$  (achieved with proper decoupling



from the low frequency vibrations), after 30 data points, the standard deviation on  $\delta\phi$  is  $\sim 3 \cdot 10^{-2}$  rad. Thus, for an interrogation time of  $T = 2$  s, the differential-acceleration resolution is  $\sim 2.5 \cdot 10^{-10}$  m·s $^{-2}$ , and the  $\eta$  parameter characterizing a test of the UFF can be measured to a precision of  $\eta \sim 5 \cdot 10^{-11}$ . For the experimental conditions encountered in a 0-g plane, an initial velocity  $v \leq 1$  cm·s $^{-1}$  and  $T = 2$  s, the effect of gravity gradients is negligible.

In conclusion, we have shown that Bayesian estimation can be efficient to perform a differential measurement between two inertial sensors using atoms of different mass and interrogation wavelength. Even for large vibrational noise, and large interrogation times, the Bayesian estimator converges rapidly. The measurement of the differential phase shift, i.e. the acceleration difference can thus be measured to a high precision. This opens new perspectives for the development of high precision test of fundamental physics such as tests of the equivalence principle. For example, we predict a precision of  $\eta \sim 5 \cdot 10^{-11}$  when using only 30 experimental data points with a free-fall time of 4 s in the Zero-G Airbus, such as for the ICE experiment [24, 25]. In the future, free-fall and integration times may be increased by deploying atom-interferometric inertial sensors on dedicated orbital platforms for next-generation tests of the UFF, at the price of an increased sensitivity to vibrational noise. The use of fast-convergence estimators will help rejecting this acceleration noise and thus relax the requirement on drag-free vibration isolation performance. A rough estimate indicates that for 20 seconds of interrogation time and an integration over 1 year [50], a target accuracy of  $\eta \sim 8 \cdot 10^{-15}$ , close to that of the project  $\mu$ SCOPE [51], is reachable with no specific drag-free platform.

## Acknowledgments

The authors would like to thank Jonas Kahn and Peter Wolf for enlightening discussions. The I.C.E. collaboration is funded by the Centre National d'Etudes Spatiales (CNES), IFRAF and RTRA "Triangle de la Physique". Further support comes from the European Union STREP consortium FINAQS and the European Space Agency MAP program A0-2004-064/082.

## Appendix A. Simple derivation of the single-atom interferometer spatial-displacement noise

It can be shown [20, 52] that the major contribution to the interferometric phase shift is due to the interaction with the Raman beams. Whenever the state of the atom changes during such an interaction, it acquires an additional phase  $\phi_i(\xi_i, t_i) = k \xi_i - \omega t_i$ . The sign of the phase depends on the initial state of the atom. The position of the atom  $\xi_i$  with respect to the retroreflecting mirror, taken at the time  $t_i$  of the pulses  $i = \{1, 2, 3\}$ , can be written  $\xi_i = \xi(t_i) = x(t_i) + \mathcal{X}(t_i)$  where  $x(t)$  is the absolute position of the atom and  $\mathcal{X}(t_i)$  is a random mirror position related to the vibration noise. Taking  $\xi_2 = t_2 = 0$ ,

$t_3 = -t_1 = T$  and tracing all the state changes leads to a phase difference

$$\phi = k[x(-T) + x(T)] + k[\mathcal{X}(-T) + \mathcal{X}(T)] \quad (\text{A.1})$$

Without gravitational field the trajectories are straightlines and the inherent symmetry of the situation leads to  $\phi = k[\mathcal{X}(-T) + \mathcal{X}(T)]$ . Here, the interferometric phase shift is only related to the vibrational noise and can be written  $\phi = \Phi = kX(T)$  where  $X(T)$  is a random variable representing the amplitude of the vibrational noise phase shift  $\Phi$  for an interrogation time  $T$ , as calculated in Appendix B.

The introduction of a gravitational field breaks the symmetry. The atom now falls three times as far during transit in the second half of the interferometer as in the first half and we find an additional contribution to the phase shift  $\phi = k a T^2$  proportional to the gravitational acceleration, so that the interferometric signal becomes :

$$n = A + B \cos(\phi + \Phi) \quad (\text{A.2})$$

## Appendix B. Interferometric phase noise of the two-species accelerometer

In this section, we derive the vernier scale relation in Eq. (5) between the interferometric phase noise standard deviations of the two-species (K-Rb) and one-species (Rb) accelerometers. Following [29, 38], the interferometric phase noise can be written

$$\Phi = \int_{-\infty}^{+\infty} h(t) \frac{d(k\mathcal{X}(t))}{dt} dt, \quad (\text{B.1})$$

where  $h(t)$  is the sensitivity function of the interferometer (see reference [29] for its definition) and  $\mathcal{X}(t)$  represents the retroreflecting mirror position at time  $t$  so that  $d^2\mathcal{X}(t)/dt^2 = \alpha(t)$  with  $\alpha(t)$  the acceleration noise of the experimental platform. Integrating by parts equation (B.1) leads to

$$\Phi = \left[ f(t) \frac{d(k\mathcal{X}(t))}{dt} \right]_{-\infty}^{+\infty} - \int_{-\infty}^{+\infty} k f(t) \alpha(t) dt, \quad (\text{B.2})$$

with  $k f(t) = \int_0^t k h(u) du$ . Neglecting the duration of the Raman light pulses ( $\tau \sim 20\mu s$  typically) with respect to the interrogation time ( $T \sim 2s$ ), the function  $h(t)$  is an odd and piecewise constant function and the function  $f(t)$  is an even and piecewise linear function; moreover,  $h(t)$  and  $f(t)$  are equal to zero out of the window  $[-T, T]$ . Thus, the first term in the above equation vanishes and the variance of the interferometric phase noise can be written:

$$\sigma_\Phi^2 = \langle \Phi^2 \rangle = \iint_{-\infty}^{+\infty} dt_1 dt_2 k f(t_1) k f(t_2) \langle \alpha(t_1) \alpha(t_2) \rangle. \quad (\text{B.3})$$

Assuming a white acceleration noise, i.e.  $\langle \alpha(t_1) \alpha(t_2) \rangle = S_\alpha^0 \delta(t_1 - t_2)$  results in a major simplification of equation (B.3), and a straightforward single-integration of  $f(t)^2$  finally leads to:

$$\sigma_\Phi^2 = (\sigma_X/k)^2 = 2k^2 T^3 S_\alpha^0 / 3 \quad (\text{B.4})$$

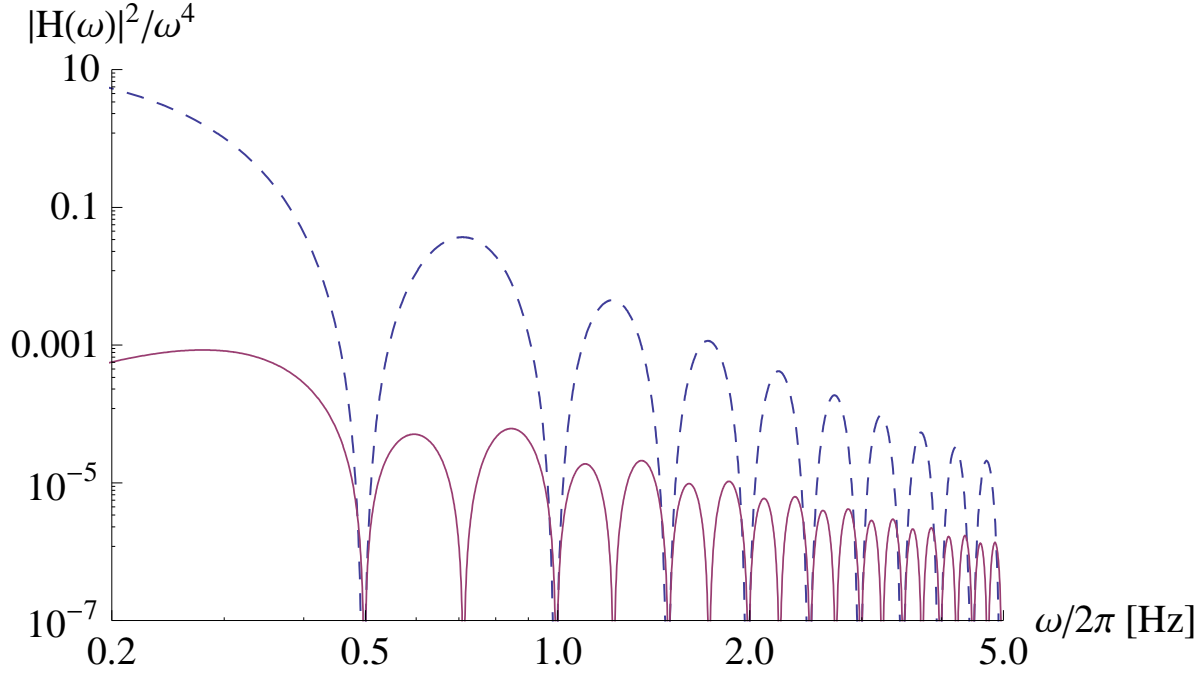


**Figure B1.** Comparison of the transfer functions of the two-species (K-Rb) and one-species (Rb, dashed line) accelerometers in the low frequency range for  $T = 2$  s.

In the case of a differential acceleration measurement, the two interferometers have different sensitivities  $h_K(t)$  and  $h_{Rb}(t)$  (because  $T_K \neq T_{Rb}$ ). Additionally, the impact of the acceleration noise is slightly different on the K-interferometer ( $\propto k_K \mathcal{X}(t)$ ) and on the Rb-interferometer ( $\propto k_{Rb} \mathcal{X}(t)$ ). The relative interferometric phase noise  $\Delta\Phi = \Phi_K - \Phi_{Rb}$  can be easily calculated by replacing  $k f(t)$  by  $k_K f_K(t) - k_{Rb} f_{Rb}(t)$  in Eq. (B.3). We find to leading order in  $\delta k/k \approx 0.017$ :

$$\sigma_{\Delta\Phi}^2 = \frac{2k^2 T^3 S_\alpha^0}{3} \left(\frac{\delta k}{2k}\right)^2 + \mathcal{O}\left(\frac{\delta k}{k}\right)^3. \quad (\text{B.5})$$

Combining Eq. (B.5) and Eq. (B.4), we can estimate the vibration noise rejection ratio between the one-species and the two-species interferometer:

$$\frac{\sigma_{\tilde{X}}}{\sigma_X} = \frac{k_K \sigma_{\Delta\Phi}}{k_K \sigma_\Phi} \approx \frac{\delta k}{2k} \approx 0.00852. \quad (\text{B.6})$$

It is also interesting to visualize this noise rejection of the two-species interferometer in the frequency domain since one often has access to the acceleration noise spectrum of the experimental platform. In this formalism, the interferometer sensitivity functions  $H_K(\omega)$  and  $H_{Rb}(\omega)$  result from the Fourier transforms of  $h_K(t)$  and  $h_{Rb}(t)$ . The variance of the relative interferometric phase noise can be written:

$$\sigma_{\Delta\Phi}^2 = \int_0^{+\infty} |H(\omega)|^2 \frac{S_\alpha(\omega)}{\omega^4} \frac{d\omega}{2\pi}, \quad (\text{B.7})$$

with  $S_\alpha(\omega)$  the acceleration noise PSD and  $H(\omega) = H_K(\omega) - H_{Rb}(\omega)$  the transfer function of the differential interferometer. In figure B1, we have plotted  $|H(\omega)|^2/\omega^4$  and the transfer function  $|H_{Rb}(\omega)|^2/\omega^4$  of a one-species (Rb) interferometer, for perfect

$\pi/2$  pulses, an effective Rabi frequency  $\Omega = 2\pi \times 50\text{kHz}$  of the Raman transitions and  $T = 2$  s. This figure shows that the relative phase noise  $\Delta\Phi$  is considerably reduced with respect to the phase noise of a single interferometer in the low frequency domain. This feature is all the more interesting that the amplitude of the acceleration noise of the platform (such as the Zero-G Airbus) is usually the highest at low frequencies.

### Appendix C. Noise rejection ratio in the aircraft A300-0G experimental platform

In this appendix we evaluate the noise rejection of the two-species accelerometer in the experimental platform where the I.C.E. experiment is performed, namely the A300-0G aircraft carrying out parabolic flights. We take into account the measured acceleration noise spectrum  $S_\alpha(\omega)$  in the plane during the quiet part of the parabola, in the direction of the Raman beams propagation. With the notations introduced in Appendix B, the noise rejection ratio is now given by

$$\frac{\sigma_{\tilde{X}}}{\sigma_X} = \frac{\sigma_{\Delta\Phi}}{\sigma_\Phi} = \left[ \frac{\int_0^{+\infty} d\omega |H(\omega)|^2 S_\alpha(\omega)/\omega^4}{\int_0^{+\infty} d\omega |H_K(\omega)|^2 S_\alpha(\omega)/\omega^4} \right]^{1/2}, \quad (\text{C.1})$$

with  $H(\omega)$  the transfer function of the differential accelerometer ( $H_K(\omega)$  for the K-accelerometer).

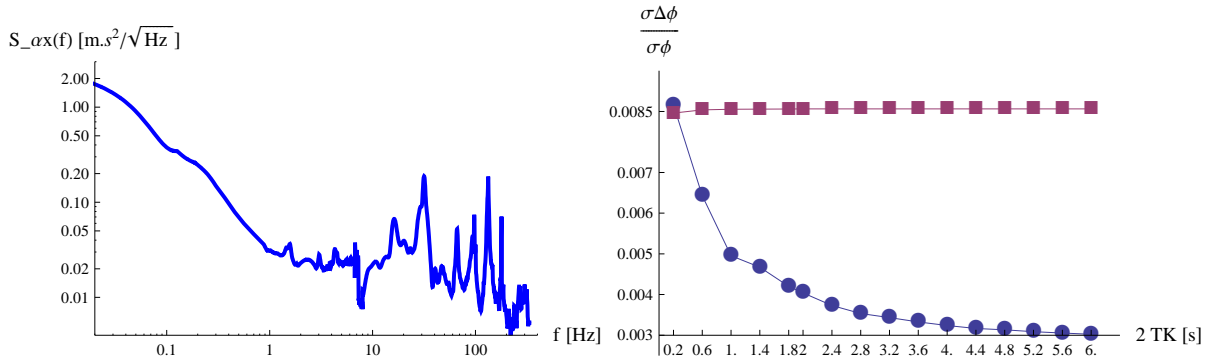


**Figure C1.** Left : measured acceleration noise spectrum of the A300-0G aircraft in the direction of the Raman beams. Right : noise rejection ratio between the one-species and the differential accelerometers for various interrogation times  $T_K$  (various scale factors). The squares correspond to a white acceleration noise whereas the dots account for the real noise spectrum in the plane.

In figure C1, we have plotted the evolution of the rejection ratio with the total interrogation time of the interferometer. We obtained these data by numerical integrations in equation (C.1), performed on one hand for the real acceleration noise in the plane, and on the other hand for a white noise ( $S_\alpha(\omega) = S_\alpha^0$ ). In the case of a white acceleration noise, we find that the noise rejection ratio is independant of the interrogation time and is equal to the vernier factor  $\delta k/2k \approx 0.0085$ , as it was derived in Appendix B. This rejection ratio can be seen as the weighted average rejection on a

limited bandwidth around  $1/T$  which contributes the most to the interferometric phase noise. When  $T$  is increased, this bandwidth shifts to lower frequencies together with the rejection efficiency. On a white noise, this leads to a constant rejection ratio. On a structured noise such as the real noise spectrum measured in the plane (figure C1), this is no longer true. For  $T_K = 100$  ms, the relevant bandwidth is around 10 Hz where the spectrum is relatively flat and we find a rejection similar to the white spectrum case. For larger values of  $T_K$ , the noise spectrum gives more weight to the low frequencies for which rejection is more efficient. The rejection ratio is then improved up to a factor 3 as one can see in figure C1. In other words, both accelerometers (one species and two-species) operate where the noise is stronger for longer  $T$ , but the two-species accelerometer phase noise will increase less than the one-species one.

## References

- [1] C. M. Will. The confrontation between general relativity and experiment. *Living Reviews in Relativity*, 9(3), 2006.
- [2] C. Lämmerzahl. The search for quantum gravity effects I. *Appl. Phys. B*, 84:551–562, September 2006.
- [3] P. Wolf, F. Chapelet, S. Bize *et al.* Cold Atom Clock Test of Lorentz Invariance in the Matter Sector. *Phys. Rev. Lett.*, 96(6):060801, February 2006.
- [4] N. Ashby, T. P. Heavner, S. R. Jefferts *et al.* Testing local position invariance with four cesium-fountain primary frequency standards and four NIST hydrogen masers. *Phys. Rev. Lett.*, 98(7):070802, 2007.
- [5] S. Blatt, A. D. Ludlow, G. K. Campbell *et al.* New limits on coupling of fundamental constants to gravity using [sup 87]sr optical lattice clocks. *Phys. Rev. Lett.*, 100(14):140801, 2008.
- [6] H. Muller, P. L. Stanwix, M. E. Tobar *et al.* Tests of relativity by complementary rotating michelson-morley experiments. *Phys. Rev. Lett.*, 99(5):050401, 2007.
- [7] T. Damour. Testing the equivalence principle: why and how? *Class. Quantum Grav.*, 13:A33–A41, November 1996.
- [8] M. Kasevich and S. Chu. Atomic interferometry using stimulated Raman transitions. *Phys. Rev. Lett.*, 67:181–184, July 1991.
- [9] J. K. Stockton, X. Wu, and M. A. Kasevich. Bayesian estimation of differential interferometer phase. *Phys. Rev. A*, 76(3):033613, 2007.
- [10] S. Dimopoulos, P. W. Graham, J. M. Hogan *et al.* Testing general relativity with atom interferometry. *Phys. Rev. Lett.*, 98(11):111102, 2007.
- [11] T. Damour, F. Piazza, and G. Veneziano. Violations of the equivalence principle in a dilaton-runaway scenario. *Phys. Rev. D*, 66(4):046007, Aug 2002.
- [12] H. B. Sandvik, J. D. Barrow, and J. Magueijo. A simple cosmology with a varying fine structure constant. *Phys. Rev. Lett.*, 88(3):031302, Jan 2002.
- [13] C. Wetterich. Probing quintessence with time variation of couplings. *Journal of Cosmology and Astro-Particle Physics*, 10:2, October 2003.
- [14] J. G. Williams, S. G. Turyshev, and D. H. Boggs. Progress in lunar laser ranging tests of relativistic gravity. *Phys. Rev. Lett.*, 93(26):261101, Dec 2004.
- [15] S. Schlamminger, K.-Y. Choi, T. A. Wagner *et al.* Test of the equivalence principle using a rotating torsion balance. *Phys. Rev. Lett.*, 100(4):041101, 2008.
- [16] K. Kuroda and N. Mio. Test of a composition-dependent force by a free-fall interferometer. *Phys. Rev. Lett.*, 62:1941–1944, April 1989.
- [17] J. Audretsch, F. W. Hehl, and C. Lämmerzahl. Matter Wave Interferometry and Why Quantum Objects are Fundamental for Establishing a Gravitational Theory. In J. Ehlers and G. Schäfer,

- editors, *Relativistic Gravity Research*, volume 410 of *Lecture Notes in Physics*, Berlin Springer Verlag, page 368, 1992.
- [18] G. Z. Adunas, E. Rodriguez-Milla, and D. V. Ahluwalia. Probing Quantum Violations of the Equivalence Principle. *General Relativity and Gravitation*, 33:183–194, February 2001.
  - [19] A. Peters, K. Yeow Chung, and S. Chu. Measurement of gravitational acceleration by dropping atoms. *Nature*, 400:849, August 1999.
  - [20] A. Peters, K. Y. Chung, and S. Chu. High-precision gravity measurements using atom interferometry. *Metrologia*, 38:25–61, 2001.
  - [21] C. J. Bordé. Atomic interferometry with internal state labeling. *Phys. Lett. A*, 1989.
  - [22] C. J. Borde, J.-C. Houard, and A. Karasiewicz. Relativistic Phase Shifts for Dirac Particles Interacting with Weak Gravitational Fields in Matter-Wave Interferometers. In C. Lämmerzahl, C. W. F. Everitt, and F. W. Hehl, editors, *Gyros, Clocks, Interferometers ...: Testing Relativistic Gravity in Space*, volume 562 of *Lecture Notes in Physics*, Berlin Springer Verlag, page 403, 2001.
  - [23] S. Fray, C. A. Diez, T. W. Hänsch *et al.* Atomic Interferometer with Amplitude Gratings of Light and Its Applications to Atom Based Tests of the Equivalence Principle. *Phys. Rev. Lett.*, 93(24):240404, December 2004.
  - [24] R. A. Nyman, G. Varoquaux, F. Lienhart *et al.* I.C.E.: a transportable atomic inertial sensor for test in microgravity. *Appl. Phys. B*, 84:673–681, September 2006.
  - [25] G. Stern, B. Battelier, R. Geiger *et al.* Light-pulse atom interferometry in microgravity. *Euro. Phys. Journ. D*, 53(3), 353-357, 2009.
  - [26] A. Vogel, M. Schmidt, K. Sengstock *et al.* Bose Einstein condensates in microgravity. *Appl. Phys. B*, 84:663–671, September 2006.
  - [27] T. Könemann, W. Brinkmann, E. Göklü *et al.* A freely falling magneto-optical trap drop tower experiment. *App. Phys. B*, 89:431–438, December 2007.
  - [28] L. Cacciapuoti, N. Dimarcq, G. Santarelli *et al.* Atomic Clock Ensemble in Space: Scientific Objectives and Mission Status. *Nuclear Physics B Proceedings Supplements*, 166:303–306, April 2007.
  - [29] P. Cheinet, B. Canuel, F. Pereira Dos Santos *et al.* Measurement of the sensitivity function in time-domain atomic interferometer. *IEEE Trans. Instr. Meas.*, pages 1141–1148, 2008.
  - [30] G. Varoquaux, N. Zahzam, W. Chaibi *et al.* I.C.E.: An Ultra-Cold Atom Source for Long-Baseline Interferometric Inertial Sensors in Reduced Gravity. In J. Dumarchez and J. T. T. Ván, editors, *Proceedings of the XLIIInd Rencontres de Moriond, Gravitational Waves and Experimental Gravity*, page 335, 2007.
  - [31] N. J. Penley, C. P. Schafer, and J.-D. F. Bartoe. The international space station as a microgravity research platform. *Acta Astronautica*, 50:691–696, June 2002.
  - [32] M. J. Snadden, J. M. McGuirk, P. Bouyer *et al.* Measurement of the earth’s gravity gradient with an atom interferometer-based gravity gradiometer. *Phys. Rev. Lett.*, 81(5):971–974, Aug 1998.
  - [33] A. Bertoldi, G. Lamporesi, L. Cacciapuoti *et al.* Atom interferometry gravity-gradiometer for the determination of the newtonian gravitational constant  $g$ . *The European Physical Journal D*, 40(2):271–279, nov 2006.
  - [34] S. Herrmann, S. wey Chiow, S. Chu *et al.* Noise-immune conjugate large-area atomm interferometers. 2009.
  - [35] C. J. Bordé. Theoretical tools for atom optics and interferometry. *Comptes Rendus de l’Académie des Sciences*, t. 2, IV:509–530, 2001.
  - [36] J. Le Gouet, T. Mehlstaubler, J. Kim *et al.* Limits to the sensitivity of a low noise compact atomic gravimeter. *App. Phys. B*, 92:133–144, 2008.
  - [37] J. Le Gouët, P. Cheinet, J. Kim *et al.* Influence of lasers propagation delay on the sensitivity of atom interferometers. *Eur. Phys. Jour. D*, 44:419–425, September 2007.
  - [38] P. Cheinet. *Conception et réalisation d’un gravimètre à atomes froids*. PhD thesis, SYRTE, Université Pierre et Marie Curie - Paris VI, 2006.
  - [39] J. Fils, F. Leduc, P. Bouyer *et al.* Influence of optical aberrations in an atomic gyroscope. *European*

- Physical Journal D*, 36:257–260, December 2005.
- [40] L. Wasserman. *All of statistics*. Springer, 2004.
  - [41] M. Zawisky, Y. Hasegawa, H. Rauch *et al.* Phase estimation in interferometry. *Jour. Phys. A*, 31:551–564, January 1998.
  - [42] G. T. Foster, J. B. Fixler, J. M. McGuirk *et al.* Method of phase extraction between coupled atom interferometers using ellipse-specific fitting. *Optics Letters*, 27:951–953, June 2002.
  - [43] C. Guerlin, J. Bernu, S. Deléglise *et al.* Progressive field-state collapse and quantum non-demolition photon counting. *Nature*, 448:889–893, August 2007.
  - [44] R. J. Dupuis and G. Woan. Bayesian estimation of pulsar parameters from gravitational wave data. *Phys. Rev. D*, 72(10):102002, November 2005.
  - [45] T. Gaiffe. From R&D brassboards to navigation grade fog-based instruments : the experience of photonetics/ixsea. *Optical Fiber Sensors Conference Technical Digest, OFS 15th*, 1:1–4, 2002.
  - [46] T. Bayes. An Essay towards solving a Problem in the Doctrine of Chances. *Philosophical Transactions of the Royal Society of London* 53: 370418, 1763)
  - [47] F. Yver-Leduc, P. Cheinet, J. Fils *et al.* Reaching the quantum noise limit in a high-sensitivity cold-atom inertial sensor. *Journal of Optics B*, 5:136, April 2003.
  - [48] P. Wolf and P. Tournenc. Gravimetry using atom interferometers: Some systematic effects. *Phys. Lett. A*, 251:241–246, January 1999.
  - [49] Ch. J. Bordé. Atomic clocks and inertial sensors. *Metrologia*, 39:435–463, 2002.
  - [50] W. Ertmer, M. Gilowski, S. Jöllenbeck *et al.* Matter Wave Explorer of Gravity (MWXG). *Experimental Astronomy*, 23(2), 2009.
  - [51] P. Touboul, M. Rodrigues, G. Métris *et al.* Microscope, testing the equivalence principle in space. *C. R. Acad. Sc (Paris)*, IV:1271–1286, 2001.
  - [52] P. Storey and C. Cohen-Tannoudji. The Feynman path integral approach to atomic interferometry: a tutorial. *Journal de Physique II*, 4:1999–2027, November 1994.